Approximate mode-based simulation of the wind turbine blade vibrations using simplified beam model

N. Navadeh[a], I.O. Goroshko[b], Y.A. Zhuk[b], A.S. Fallah[a,c,d]

[a] ACEX Building, Department of Aeronautics, South Kensington Campus, Imperial College London, London SW7 2AZ, UK
[b] Department of Theoretical and Applied Mechanics, Taras Shevchenko National University of Kyiv, Kiev 01601, Ukraine
[c] Howell Building, Department of Mechanical and Aerospace Engineering, Brunel University London, Uxbridge UB8 3PH, UK
[d] Institute of Computational Physics, Zürich University of Applied Sciences (ZHAW), 21 Wildbachstrasse, Winterthur 8401, Switzerland

Abstract.

In this paper work the questions of the simulation of the wind turbine blade dynamics on the basis numerical realization of the developed low dimensional beam type model are considered. From the governing system of differential-algebraic equations of the simplified beam type model of the blade, using the mode superposition approximation, the system of linear ordinary differential equations with respect to the coefficient functions of the modal representation was obtained. The developed program codes allow to simulate low frequency bending vibrations of wind turbine blades under different stationary and transient loadings. The comparison of the simulation results obtained by the proposed simplified blade model with the results of the direct FEM simulation shows their close agreement, that confirm an adequacy of the developed model and its mode-based approximation to the engineering practice requirements. The presented approach to the creating low-dimensional simplified models of slender structures can be useful in different fields of aerospace, civil and transport engineering.

1. Introduction

Development of modern wind turbines and control of their dynamics in different operation modes need intensive computer simulation of vibrations of critical elements as rotor blades. Nowadays wind turbine blades are designed as long (tens meters) slender composite shell structures with stiffeners, significantly inhomogeneous (slenderising towards the end). Modern FEM packages like ANSYS, ABAQUS etc. allow to simulate mechanical processes in such turbine blades with high accuracy (Chen & Chen, 2010), but in many cases, e.g. investigation of general structural dynamics, aero-elastic vibrations, preliminary design and model based vibration control, such detailed models are redundant and can be replaced by simplified one-dimensional beam type models which allow to describe general blade deformations with appropriate accuracy and require much less simulation time or computational resources.

Parameters of the required simplified beam models (SBM) are derived from results of physical or numerical (detailed FEM computations) experiments using different equivalenting and identification techniques. This approach is widely used for different aerospace structures (wings, fuselages, etc.) (Lee, 1995; Malcolm & Laird, 2003; Malcolm & Laird, 2007; Trivailo et al., 2006; Stodieck et al., 2018).

But in the case of the wind turbine blades the situation is complicated due to considerable structure pre-twisting that doesn't allow to split flap and lead-lag motions in mathematical model.

In previous article (Navadeh et al., 2017) an approach to construction of a beam type simplified model of a horizontal axis wind turbine (HAWT) composite blade based on the results of more detailed finite element method (FEM) simulations of the blade was proposed. The parameters of the model are obtained using identification procedure from the FEM modal analysis data. This model allows effective description of low vibration bending modes of the blade taking into account the effects of coupling between flap wise and lead-lag vibrations. The present paper is devoted to simulation of transient

vibrations of the wind turbine blade using the simplified model on the basis of the mode superposition method and evaluation of its effectiveness by comparison with the results of computations for the original shell type FEM model.

2. Low-dimensional simplified beam-mass model of turbine blade

The real wind turbine blade is approximated by a piecewise homogeneous cantilever beam consisting of N weightless sections of length L_k with lumped masses $m_k, k = \overline{1, N}$, located at the connection points between sections and at the end point, as shown in Figure 1. To take into account the distribution of twist angle in the blade geometry along its length, principal axes of beam segment scross-sections x_k, y_k are rotated around longitudinal axis z by angles α_k (see Figure 2). The$y$-axis is oriented in the flap direction and the x-axis is in lead-lag bending direction. The x and y axes of the global coordinate system is oriented in the turbine rotor plane (lead-lag) and orthogonal to it(flap) directions respectively.

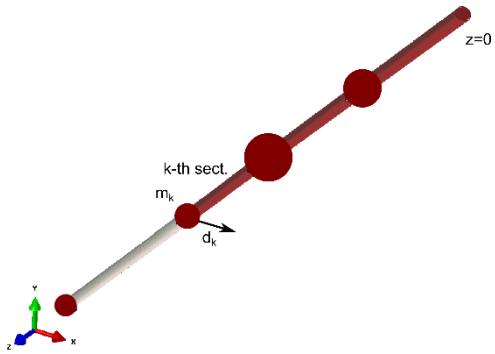

Figure 1. Structure of the simplified beam-mass blade model

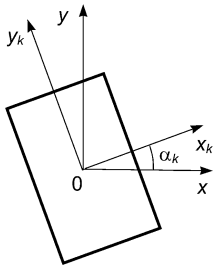

Figure 2

The deformation of each beam section in local coordinates is described by standard Euler-Bernoulli equations:

$$(EI_y)_k \frac{\partial^4 u_k}{\partial z^4} = 0 \quad \text{and} \quad (EI_x)_k \frac{\partial^4 v_k}{\partial z^4} = 0, \tag{1}$$

where $(EI_y)_k$ and $(EI_x)_k$ are bending stiffnesses. Since the beam sections are connected to masses and are parts of the dynamic system, displacement components depend not only on z coordinate, but also on

time t: $u_k = u_k(z,t)$, $v_k = v_k(z,t)$. Thus, we are dealing with a discrete parameter model in which lumped masses are connected by beam elements with distributed stiffnesses described by equations (1).

In the beam elements displacements u_k, v_k are presented by general solutions of homogeneous differential equations (1) which are polynomials of the third order. Using local coordinate ξ_k (measured from the beginning of the section in z direction), they can be written as:

$$u_k = a_0^{(k)} + a_1^{(k)}\xi_k + a_2^{(k)}\xi_k^2 + a_3^{(k)}\xi_k^3,$$
$$v_k = b_0^{(k)} + b_1^{(k)}\xi_k + b_2^{(k)}\xi_k^2 + b_3^{(k)}\xi_k^3. \quad (2)$$

As the generalized coordinated for the components of displacements, the coefficients $a_j^{(k)}$ and $b_j^{(k)}$ in (2) also are functions of time.

The components of basis unit vectors of the k-th local coordinate system in the reference global coordinate system (subscript "0") are presented as:

$$\mathbf{e}_x^{(k)} = (\cos\alpha_k, \sin\alpha_k)_0, \ \mathbf{e}_y^{(k)} = (-\sin\alpha_k, \cos\alpha_k)_0, \quad (3)$$

and for the components of displacement vector for the k-th beam section in the global coordinate system we have

$$\mathbf{u}_k = u_k\mathbf{e}_x^{(k)} + v_k\mathbf{e}_y^{(k)} = (u_k\cos\alpha_k - v_k\sin\alpha_k, \ u_k\sin\alpha_k + v_k\cos\alpha_k)_0. \quad (4)$$

Such transformations are universal and affect the components of any other vectors, such as moments and forces.

At the points of connection between sections continuity conditions are hold i.e. the components, in the global coordinate system, of transversal displacements and their derivatives with respect to z(rotations) as well as components of bending moments are continuous. The components of shear forces have jumps due to the applied external forces and inertial forces from the lumped masses. At the end free tip point, zero moment and shear force–inertial force conditions hold. At the clamped point of the beam (z=0), the cantilever beam essential boundary conditions hold which give for the coefficients of the beam solutions (2) $a_0^{(1)} = a_1^{(1)} = b_0^{(1)} = b_1^{(1)} = 0$. The conditions for displacements, rotations and moments have the form of linear algebraic equations, whereas the dynamic force conditions and ordinary differential equations. Together with expressions for the displacement components at the end point in global coordinate system u_{END}, v_{END} these equations form linear differential-algebraic (DAE) system with respect to components of the vector of governing functions of the problem

$$c(t) = \left\{\{a_j^k\}_{k=0}^N, \{b_j^k\}_{k=0}^N, u_{END}, v_{END}\right\}. \quad (5)$$

In the previous article (Navadeh et al., 2017) only free vibrations were considered, and the components of external forces applied to the lumped masses were omitted, thus the governing system of equations was homogeneous and in matrix notations had the form

$$Ac = B\ddot{c} \quad (6)$$

where A and B are square and rectangular matrixes of constant coefficients respectively. The detailed representation of the governing system of equations in expanded formis given in (Navadeh et al., 2017).

To obtain natural frequencies and shapes of vibration modes for the simplified beam-mass blade model the solutions of (6) are represented in exponential form $c(t)=\bar{c}e^{\lambda t}$, that leads to solving the generalized eigenvalue problem (Gruber, 2014)

$$A\bar{c}=\lambda^2 B\bar{c}\,, \tag{7}$$

which gives the spectrum of eigenvalues, λ_k^2, and corresponding eigenvectors c_k. The natural cyclic frequencies of vibrations are calculated by the formulae $f_k=\sqrt{-\lambda_k^2}/(2\pi)$, and components of the c_k vectors are used to represent shapes of the normal vibration modes by equations (2).

Note that in (Navadeh et al., 2017) the differential equations of the governing system, which are the component expressions in global coordinates of the second Newton's law for the first $N-1$ lumped masses of the considered beam-mass model, were not solved with respect to the higher-order (second)time derivatives of the $a_0^{k+1}, b_0^{k+1},\ k=\overline{1,N-1}$, which are the components of displacements in local coordinate systems at the connection points between beam sections (see eqn. (2)), i.e. the displacement components for the corresponding *k*-th masses. It's not convenient for the further analysis, and these equations should be transformed into a simpler form.

From the conditions of the force balance at connection points between beam segments ($k=\overline{1,N-1}$) (eqn. (7), (8) in (Navadeh et al., 2017)) and taking into account components $F_x^{(k)}(t), F_y^{(k)}(t)$ of external forces applied at these points, we have following dynamic equations (hereinafter dots denote temporal differentiation):

$$\begin{aligned} &m_k(\ddot{a}_0^{(k+1)}\cos\alpha_{k+1}-\ddot{b}_0^{(k+1)}\sin\alpha_{k+1})=F_x^{(k)}(t)\\ &\quad+6a_3^{(k)}(EI_y)_k\cos\alpha_k-6a_3^{(k+1)}(EI_y)_{k+1}\cos\alpha_{k+1}-6b_3^{(k)}(EI_x)_k\sin\alpha_k+6b_3^{(k+1)}(EI_x)_{k+1}\sin\alpha_{k+1}, \end{aligned} \tag{8}$$

$$\begin{aligned} &m_k(\ddot{a}_0^{(k+1)}\sin\alpha_{k+1}+\ddot{b}_0^{(k+1)}\cos\alpha_{k+1})=F_y^{(k)}(t)\\ &\quad+6a_3^{(k)}(EI_y)_k\sin\alpha_k-6a_3^{(k+1)}(EI_y)_{k+1}\sin\alpha_{k+1}+6b_3^{(k)}(EI_x)_k\cos\alpha_k-6b_3^{(k+1)}(EI_x)_{k+1}\cos\alpha_{k+1}. \end{aligned} \tag{9}$$

Multiplying equation (8) by $\cos\alpha_{k+1}$ and equation (9) by $\sin\alpha_{k+1}$ and adding them, we obtain

$$\begin{aligned} &m_k\ddot{a}_0^{(k+1)}=F_x^{(k)}(t)\cos\alpha_{k+1}+F_y^{(k)}(t)\sin\alpha_{k+1}\\ &\quad+6a_3^{(k)}(EI_y)_k\cos(\alpha_k-\alpha_{k+1})-6a_3^{(k+1)}(EI_y)_{k+1}-6b_3^{(k)}(EI_x)_k\sin(\alpha_k-\alpha_{k+1}). \end{aligned} \tag{10}$$

Then, multiplying (9) by $\cos\alpha_{k+1}$ and (8) by $\sin\alpha_{k+1}$ and subtracting the second from the first, we obtain

$$\begin{aligned} &m_k\ddot{b}_0^{(k+1)}=F_y^{(k)}(t)\cos\alpha_{k+1}-F_x^{(k)}(t)\sin\alpha_{k+1}\\ &\quad+6a_3^{(k)}(EI_y)_k\sin(\alpha_k-\alpha_{k+1})+6b_3^{(k)}(EI_x)_k\cos(\alpha_k-\alpha_{k+1})-6b_3^{(k+1)}(EI_x)_{k+1}. \end{aligned} \tag{11}$$

The dynamic equations at the end point of the beam have the form (see eqn. (9) in [NaGoZhFa, 2017])

$$m_N\ddot{u}_{END}=F_x^{(N)}(t)+6a_3^{(N)}(EI_y)_N\cos\alpha_N-6b_3^{(N)}(EI_x)_N\sin\alpha_N, \tag{12}$$

$$m_N\ddot{v}_{END}=F_y^{(N)}(t)+6a_3^{(N)}(EI_y)_N\sin\alpha_N+6b_3^{(N)}(EI_x)_N\cos\alpha_N. \tag{13}$$

Since in further consideration the mode superposition method is applied, we doesn't present here sufficiently large algebraic equations which express in governing DAE system continuity conditions

(Navadeh et al., 2017), because the components of eigenvectors, used for the solution representation, satisfy these equations identically.

3. Mode superposition method for simulation of transient dynamicsof the wind turbine blade

The considered simplified beam-mass model, which parameters were obtained using the identification procedure, can effectively represent low frequency bending vibrations of the blade with structural pre-twisting (Navadeh et al., 2017). Because of this, to investigate transient deformations of the blade using this model, instead of the direct solution of the linear DAE system, which describes the dynamic behaviour of the wind turbine blade, that needs utilization of special numerical methods (and moreover can give additional errors due to the model inaccuracy in the higher frequency range), it's more effective to use the mode superposition technique.

In the framework of the mode superposition method (Bathe, 2014), the solution for the vector of governing functions $c(t)$ (5) of the linear DAE system is represented as a linear combination of eigenvectors c_m, obtained from the generalized eigenvalue problem (6), with time-dependent coefficient functions $d_m(t)$. To investigate low frequency bending vibrations of the blade we will use the superposition of only the first *M* modes in the range, where the using beam type model has sufficient agreement with more detailed FEM one:

$$c(t) \approx \sum_{m=1}^{M} d_m(t) c_m. \tag{14}$$

Substituting corresponding components of the representation (14) into dynamic equations (10)–(13), we obtain the following system of $2N$ ordinary differential equations with respect to thefunctions $d_m(t)$:

$$\begin{aligned}
&m_k \sum_{m=1}^{M} \ddot{d}_m(t) a_{0m}^{(k+1)} = F_x^{(k)}(t)\cos\alpha_{k+1} + F_y^{(k)}(t)\sin\alpha_{k+1} + \sum_{m=1}^{M} d_m(t) A_m^{(k)},\\
&m_N \sum_{m=1}^{M} \ddot{d}_m(t) u_{ENDm} = F_x^{(N)}(t) + \sum_{m=1}^{M} d_m(t) A_m^{(N)},\\
&m_k \sum_{m=1}^{M} \ddot{d}_m(t) b_{0m}^{(k+1)} = F_y^{(k)}(t)\cos\alpha_{k+1} - F_x^{(k)}(t)\sin\alpha_{k+1} + \sum_{m=1}^{M} d_m(t) B_m^{(k)},\\
&m_N \sum_{m=1}^{M} \ddot{d}_m(t) v_{ENDm} = F_y^{(N)}(t) + \sum_{m=1}^{M} d_m(t) B_m^{N}.
\end{aligned} \tag{15}$$

Here $k = \overline{1, N-1}$, $a_{0m}^{(k+1)}$, $b_{0m}^{(k+1)}$, u_{ENDm}, v_{ENDm} are components of the *m*-th eigenvector c_m, and

$$\begin{aligned}
&A_m^{(k)} = 6a_{3m}^{(k)}(EI_y)_k \cos(\alpha_k - \alpha_{k+1}) - 6a_{3m}^{(k+1)}(EI_y)_{k+1} - 6b_{3m}^{(k)}(EI_x)_k \sin(\alpha_k - \alpha_{k+1}),\\
&A_m^{(N)} = 6a_{3m}^{(N)}(EI_y)_N \cos\alpha_N - 6b_{3m}^{(N)}(EI_x)_N \sin\alpha_N,\\
&B_m^{(k)} = 6a_{3m}^{(k)}(EI_y)_k \sin(\alpha_k - \alpha_{k+1}) + 6b_{3m}^{(k)}(EI_x)_k \cos(\alpha_k - \alpha_{k+1}) - 6b_{3m}^{(k+1)}(EI_x)_{k+1},\\
&B_m^{(N)} = 6a_{3m}^{(N)}(EI_y)_N \sin\alpha_N + 6b_{3m}^{(N)}(EI_x)_N \cos\alpha_N.
\end{aligned} \tag{16}$$

Then, using the Galerkin projection technique, we multiply equations in (15) by corresponding components of *j*-th($j = \overline{1, M}$) eigenvectors used for the solution approximation (14) and sum them. As the result we obtain M ordinary differential equations with respect to M coefficient functions $d_m(t)$:

$$\sum_{k=1}^{N-1} m_k \sum_{m=1}^{M} \ddot{d}_m(t) a_{0m}^{(k+1)} a_{0j}^{(k+1)} + m_N \sum_{m=1}^{M} \ddot{d}_m(t) u_{ENDm} u_{ENDj}$$
$$+ \sum_{k=1}^{N-1} m_k \sum_{m=1}^{M} \ddot{d}_m(t) b_{0m}^{(k+1)} b_{0j}^{(k+1)} + m_N \sum_{m=1}^{M} \ddot{d}_m(t) v_{ENDm} v_{ENDj} =$$
$$\sum_{m=1}^{M} \ddot{d}_m(t) \left[\sum_{k=1}^{N-1} m_k a_{0m}^{(k+1)} a_{0j}^{(k+1)} + m_N u_{ENDm} u_{ENDj} + \sum_{k=1}^{N-1} m_k b_{0m}^{(k+1)} b_{0j}^{(k+1)} + m_N v_{ENDm} v_{ENDj} \right] =$$
$$\sum_{m=1}^{M} d_m(t) \left[\sum_{k=1}^{N-1} A_m^{(k)} a_{0j}^{(k+1)} + A_m^{(N)} u_{ENDj} + \sum_{k=1}^{N-1} B_m^{(k)} b_{0j}^{(k+1)} + B_m^{(N)} v_{ENDj} \right]$$
$$+ \sum_{k=1}^{N-1} (F_x^{(k)}(t) \cos\alpha_{k+1} + F_y^{(k)}(t) \sin\alpha_{k+1}) a_{0j}^{(k+1)} + F_x^N(t) u_{ENDj} \tag{17}$$
$$+ \sum_{k=1}^{N-1} (F_y^{(k)}(t) \cos\alpha_{k+1} - F_x^{(k)}(t) \sin\alpha_{k+1}) b_{0j}^{(k+1)} + F_y^N(t) v_{ENDj}.$$

Due to the orthogonality of displacements in eigenvectors with mass weights we have

$$\sum_{m=1}^{M} \ddot{d}_m(t) \left[\sum_{k=1}^{N-1} m_k a_{0m}^{(k+1)} a_{0j}^{(k+1)} + m_N u_{ENDm} u_{ENDj} + \sum_{k=1}^{N-1} m_k b_{0m}^{(k+1)} b_{0j}^{(k+1)} + m_N v_{ENDm} v_{ENDj} \right] =$$
$$\ddot{d}_j(t) \left[\sum_{k=1}^{N-1} m_k (a_{0j}^{(k+1)})^2 + m_N u_{ENDj}^2 + \sum_{k=1}^{N-1} m_k (b_{0j}^{(k+1)})^2 + m_N v_{ENDj}^2 \right], \tag{18}$$

that simplifies solving the ODE system (17), because its mass matrix is diagonal.

Finally, we can represent the obtained ODE system (17) in the matrix-vector form, convenient for further numerical analysis (Bathe, 2014):

$$\ddot{\mathbf{d}} = \mathbf{P}^{-1}\mathbf{Q}\mathbf{d} + \mathbf{P}^{-1}\mathbf{f}. \tag{19}$$

Here $\mathbf{d}$ is a column vector of $d_j(t)$;
the diagonal components of the mass matrix $\mathbf{P}$ are

$$P_j = \sum_{k=1}^{N-1} m_k (a_{0j}^{(k+1)})^2 + m_N u_{ENDj}^2 + \sum_{k=1}^{N-1} m_k (b_{0j}^{(k+1)})^2 + m_N v_{ENDj}^2, \tag{20}$$

i.e. $\mathbf{P} = diag(P_j)$, and $\mathbf{P}^{-1} = diag(P_j^{-1})$,
the components of the stiffness matrix $\mathbf{Q}$ have the form

$$Q_{jm} = \sum_{k=1}^{N-1} A_m^{(k)} a_{0j}^{(k+1)} + A_m^{(N)} u_{ENDj} + \sum_{k=1}^{N-1} B_m^{(k)} b_{0j}^{(k+1)} + B_m^{(N)} v_{ENDj}, \tag{21}$$

and the components of the load vector $\mathbf{f}$ are expressed as

$$f_j = \sum_{k=1}^{N-1}(F_x^{(k)}(t)\cos\alpha_{k+1} + F_y^{(k)}(t)\sin\alpha_{k+1})a_{0j}^{(k+1)} + F_x^N(t)u_{ENDj} + \sum_{k=1}^{N-1}(F_y^{(k)}(t)\cos\alpha_{k+1} - F_x^{(k)}(t)\sin\alpha_{k+1})b_{0j}^{(k+1)} + F_y^N(t)v_{ENDj}. \quad (22)$$

4. Results of numerical simulation

For simulation of the transient dynamics of the wind turbine blade using the developed multi-segment beam-mass model in the frame of the described above mode superposition approximation, and for the graphical representation of the results of computations, the Matlab codes were developed. Also for setting loads in the FEM model of the blade, developed in ABAQUS (2014), and extracting simulation results the corresponding Python scripts were written.

In the present study, as it was done in (Chen & Chen, 2010) and (Navadeh et al., 2017), the blade for the three-bladed horizontal-axis upwind turbine with a rated power of 3 MW was chosen as the reference model being investigated. In fact, this is a modified version of a 3 MW turbine proposed by researchers (Malcolm & Hansen, 2006). The rotor blade, which is 44.175 m long, has a circular cross-section at its root attaching the rotor hub to the 1.753-meter span location. Then the circular blade cross-sections gradually go through transition to airfoil sections that have NREL airfoil types of S818 at the 9.648-meter span location, S825 at 32.667-meter, and S826 at 41.873-meter and 44.175-meter (at the blade tip). These NREL types of airfoils can be seen in Fig. 1 from the paper by (Chen & Chen, 2010) along with the exact details of the 14 cross-sections forming the blade. Between these cross-section there transpires a linear transition on shape and the chord length distribution is according to that work.

In the FEM simulations conducted in ABAQUS, the reduced integration quadratic shell elements S8R with global size 200 mm were used. The thickness of the shell varies between 92.02 mm at the root to 10.34 mm at the tip of the blade. The FEM model parameters used in the paper are adopted from (Navadeh et al., 2017) where the simplified beam model parameters used here were identified.

To evaluate the effectiveness of the simplified model of the blade in comparison with the detailed FEM model we consider the vibrations of the blade under a step in time loading in *y* direction, distributed along the top reference line of the FEM model, as shown in Figure 3.The magnitude of the load density varies linearly from the value –1000 N at the root of the blade to –200 N at its end.

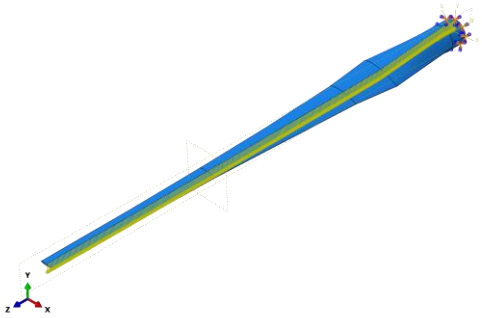

Figure3

In the present study simulations using the simplified beam model were carried out for number of segments N=6, using the model parameters obtained through the identification procedure in the previous article (Navadeh et al., 2017). The two most stiff root parts 1 and 2 were combined into one SBM part because of their large thickness. The 3rd segment of the shell structure was treated as the 3rd segment of SBM because of its intermediate thickness, and the long flexible parts 4 and 5 of different skin thickness were divided into two segments of practically equal length (see Table 1).

Coordinates of the end nodes z_k (m), length of beam segments L_k, values of bending stiffnesses EI_x and EI_y twisting angles α_k (degrees) for the k-th sections, and lumped masses m_k (kg), located at nodes, are given in Table 1:

Table 1. Beam model segment data (SI units)

k	1	2	3	4	5	6
z_k	9.648	14.251	21.7315	29.212	36.6935	44.175
L_k	9.648	4.603	7.4705	7.4805	7.4815	7.4815
$(EI_x)_k$	$7.2953\cdot10^9$	$4.0715\cdot10^8$	$1.1509\cdot10^8$	$2.3845\cdot10^7$	$8.6304\cdot10^6$	$6.7160\cdot10^6$
$(EI_y)_k$	$1.3532\cdot10^{10}$	$5.8728\cdot10^9$	$1.9179\cdot10^9$	$6.2110\cdot10^8$	$2.7655\cdot10^8$	$1.6842\cdot10^8$
α_k	-12.856	-10.263	-6.335	-3.665	-2.06	-1.52
m_k	6985.084	2003.617	$1.1509\cdot10^8$	$2.3845\cdot10^7$	$8.6304\cdot10^6$	$6.7160\cdot10^6$

In mode superposition representation of equation (14) the first four modes were used. It is worth mentioning here that in the first step, the simulations were performed by inclusion of all 6 modes identified in the paper (Navadeh et al., 2017). The results of computations carried out showed that the influence of the fifth and sixth modes is negligible; therefore, accounting for the first four modes is necessary while influence of the above mentioned 5th and 6th modes can be neglected.

The transient dynamic analysis for the shell type model in ABAQUS was fulfilled by the direct time integration.

The results of simulation for displacements (m) in the y (flap) direction at the nodes, where lumped masses are located, are shown on the time segment from 0 to 3 seconds in Figure 4 (graphs a–f correspond to consecutive k-th nodes, see Figure 1). Solid lines represent the displacements, obtained by the simplified model, whereas dashed lines represent the results of the direct FEM simulation.

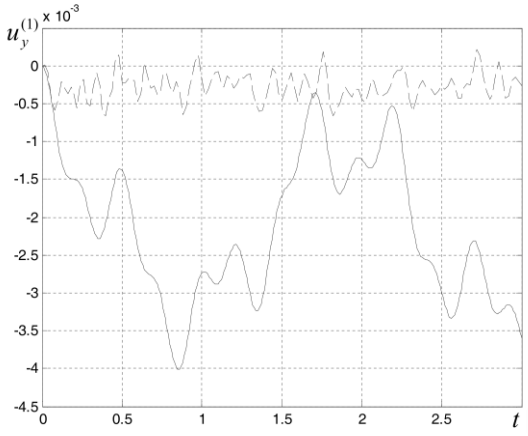

a

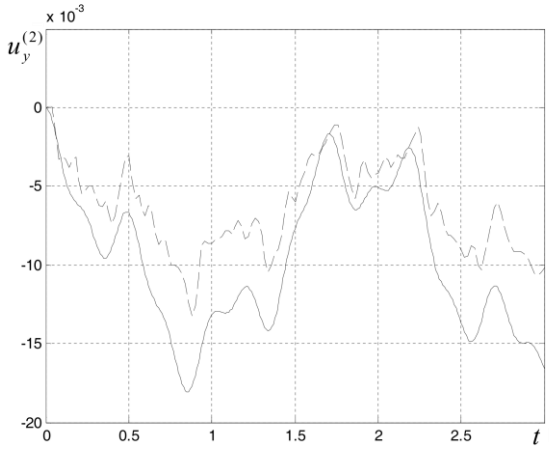

b

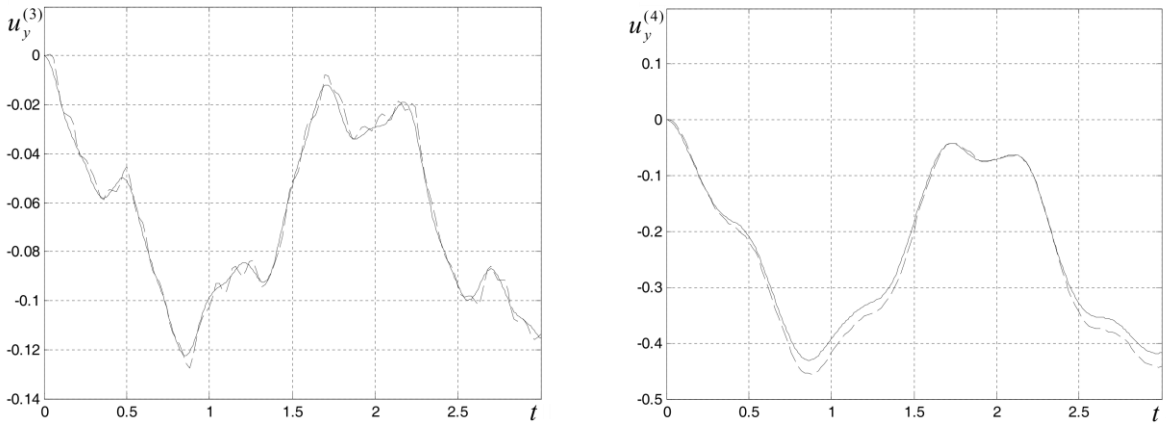

c

d

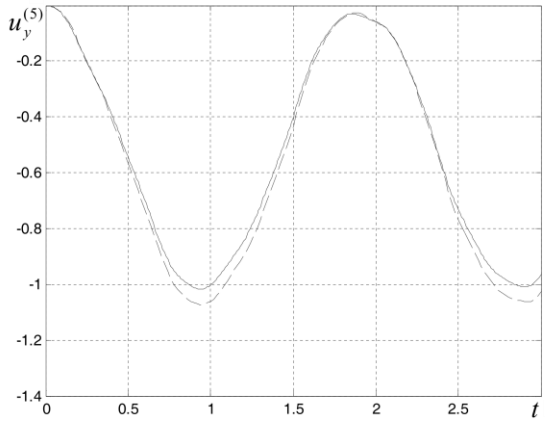

e

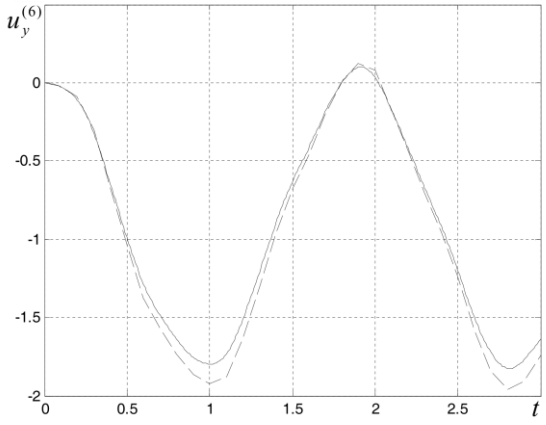

f

Figure 4

As it is seen in Figure 4.a, FEM and SBM results are not in close agreement. This occurs because the Euler–Bernoulli beam model used for SBM approximation is significantly less accurate for the first two segments of the blade (they are jointed into one segment of SBM) due to their stubby geometry i.e. relatively thick walls and short length. This effect appears not to be critical because the absolute error in the displacement in the 1st node of SBM (see Figure 4.a) is significantly less than the displacements in other nodes (see Fig. 4.b-f).

Besides, in Figure 5 the time dependencies of the coefficient functions $d_m(t)$ of the mode superposition representation (14), which define the contributions of different modes into the solution, are presented:

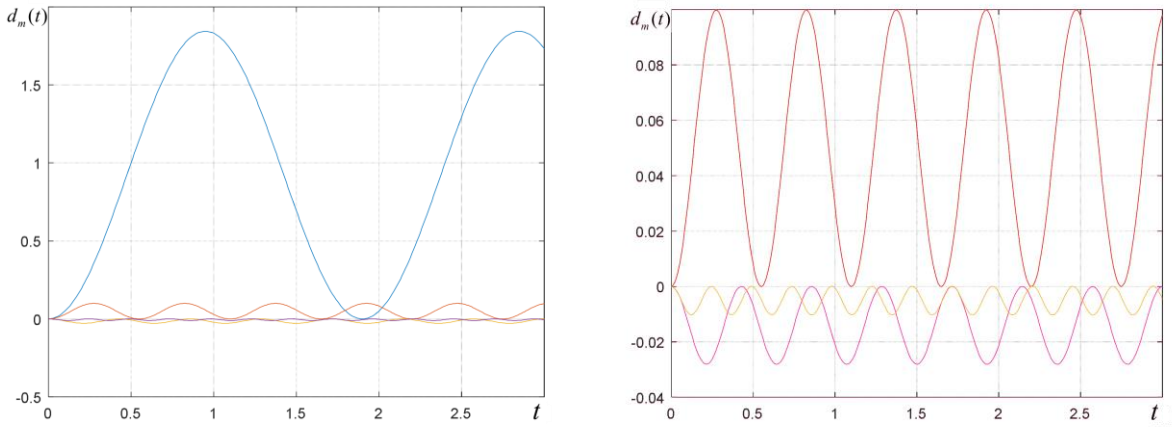

a b

Figure 5. Coefficient functions of the mode superposition representation:
a) $d_1(t)$ (blue line), $d_2(t)$ (red); b) $d_2(t)$ (red), $d_3(t)$ (magenta), $d_4(t)$ (yellow).

The comparison of the graphs in Figure 4 demonstrates a close agreement of the results, obtained by the simulation of the beam dynamic response under a step in time impulse loading, using simplified beam-type blade model, with more precise FEM ones. This indicates that the utilized four-mode approximation is adequate and allows to describe low frequency vibrations of the blade with sufficient for practical purposes accuracy.

From Figure 5 it is seen that at the considered loading the magnitude of $d_1(t)$ is almost twenty times greater then $d_2(t)$, and much more then $d_3(t)$ and $d_4(t)$. The result of this, taking into account the shapes in *y* direction of the first and second normal modes which are represented in (Navadeh et al., 2017) in Figure 5a, b, is domination of the first mode's contribution to displacements at the fifth and sixth nodes (see Figure 4e and f respectively). But at the fourth node, where the shape function of the first mode became near four times less then at the beam end, when the magnitudes of the second and third mode shape functions have absolute values some more then a half of their maximums (note that these modes have similar shapes in *y* direction, but different frequencies),as can be seen in Figure 4d,the contribution of the last modes is much more significant. Lastly, considering the graph of displacements at the third node Figure 4c we see that the presence in the used four-mode approximation of the fourth mode allow to represent motion in time more detailed then it could be done if only three modes were taken into account.

It should be noted that at the second node the displacements, obtained by the simplified beam model, are about one and a half times greater in magnitude than corresponding values computed using more detailed FEM model, but the shapes of their time dependencies remain similar. This is explained by a decrease in the accuracy of the classical beam model (1) which is used in the blade approximation. However this inaccuracy in many cases can be neglected, because the magnitude of vibrations observing here is ~1% of the maximal magnitude at the blade's end. The same can be said about the low relational accuracy of the solution by the beam approximated model at the first node, where its magnitude relatively to the magnitude of vibrations at the blade's end is ~0.2% vise <0.04% after the FEM simulation.

5. Conclusions

In the present work the questions of the simulation of the wind turbine blade dynamics on the basis numerical realization of the approximated low dimensional beam type model, which was developed in (Navadeh et al., 2017), are considered.

Primarily, the dynamic equations, that are included in the governing DAE system of the simplified mass-beam model of the blade, were transformed to ODEs, solved with respect to the higher-order time derivatives of the node displacement components of the vector of governing functions. This allows to simplify the application of the mode superposition technique for approximate simulation of transient wind turbine blade vibrations.

In the framework of the mode superposition method, the solution for the vector of governing functions of the linear DAE system was represented as a linear combination of eigenvectors, obtained from the generalized eigenvalue problem, with time-dependent coefficient functions. It should be noted that in practice for the investigation of low frequency bending vibrations of the beam type structures frequently the approximations containing only the several first vibrational modes is used, and here the number of modes is limited in the range, where the using beam type model has sufficient agreement with the real blade behaviour (described more detailed by the FEM model). As the result of substitution of the mode superposition representation into governing DAE system and utilization of the Galerkin projection technique, the linear ODE system with respect to coefficient functions was obtained. Due to orthogonality of displacements in eigenvectors with mass weights this system has diagonal mass matrix and can be solved by standard numerical methods.

For the evaluation of the accuracy of the developed simplified beam type model of the wind turbine blade with mode superposition approximation in comparison with the precise FEM model the vibrations of the blade under a step in time loading which density varies linearly along the blade were considered.

The results of simulation of the transient dynamics of the blade in the frame of the described above approximate model approach show a close agreement with the results, obtained by the direct FEM simulation, that indicates the consistency of this approach and its adequacy for the describing low frequency vibrations of wind turbine blades with sufficient for practical purposes accuracy.

Modeling and simulation approaches developed in (Navadeh et al., 2017) and in this paper can be applied not only for investigation of the wind turbine blade dynamics, but also in more wide fields of the aerospace, civil and transport engineering (vibrations, stability and model based control of wings, fuselages, space launchers, high buildings, bridges, pipelines and other long-dimensional structures).

References

ABAQUS. (2014). v. 6.14 User Guide.

Bathe, K. J. (2014). Finite Element Procedures, 2nd edition.Watertown, MA: K.J. Bathe.

Chen, K.-N., & Chen, P.-Y. (2010). Structural optimization of 3 MW wind turbine blades usinga two-step procedure. International Journal for Simulation and Multidisciplinary DesignOptimization, 4, 159–165.

Gruber, M. H. J. (2014). Matrix algebra for linear models. San Francisco, CA: Wiley.

Lee, U. (1995). Equivalent dynamic beam–rod models of aircraft wing structures. AeronauticalJournal, 99(990), 450–457.

Malcolm, D. J., & Laird, D. L. (2003). Modeling of Blades as Equivalent Beams for Aeroelastic Analysis. ASME 2003 Wind Energy Symposium. doi:10.1115/wind2003-870.

Malcolm, D. J., Hansen, A. C. (2006). WindPACT Turbine RotorDesign Study, Subcontract Report NREL/SR-500-32495, National Renewable Energy Laboratory, Golden, Colorado, USA.

Malcolm, D. J., & Laird, D. L. (2007). Extraction of equivalent beam properties from blade models, Wind Energy, 10, 135–157. DOI: 10.1002/we.213.

Navadeh, N., Goroshko, I. O., Zhuk, Y. A., & Fallah, A. S. (2017). An FEM-based AI approach to model parameter identification for low vibration modes of wind turbine composite rotor blades, European Journal of Computational Mechanics, 26(5–6), 541–556.

Stodieck O., Cooper J.E., Neild S.A., Lowenberg M.H., Iorga L. (2018) Slender-Wing Beam Reduction Method for Gradient-Based Aeroelastic Design Optimization, AIAA Journal, 56(11), 4529-4545.

Trivailo, P. M., Dulikravich, G. S., Sgarioto, D., & Gilbert, T. (2006). Inverse problem of aircraftstructural parameter estimation: Application of neural networks. Inverse Problems in Scienceand Engineering, 14(4), 351–363.